Multiple Features-Based Improved Nanohole Array Plasmonic Biosensor

Tashfiq Ahmed, *Member, IEEE*, A. K. M. Naziul Haque, and Muhammad Anisuzzaman Talukder

***Abstract*—In recent years, gold nanohole array-based biosensors have gained tremendous attention due to their high sensitivity, label-free biosensing, and real-time simultaneous multiple analyte detection capabilities. However, nanohole array-based biosensors using conventional sensing methods lack the resolution of traditional surface plasmon resonance (SPR) sensors. In this work, we present numerical methods utilizing multiple peaks of these biosensors' transmission spectra to achieve higher sensitivity and lower detection limits. Using finite-difference time-domain (FDTD) simulations, we compared the sensing performance of the proposed numerical methods to traditional peak-shift and spectral integration methods. We added noise to the transmission spectra to simulate a realistic system and determined the change in the performance. We also optimized the geometrical parameters of the gold nanohole array for optimal sensing performance. Finally, we applied the proposed method to two critical real-life biosensing applications and reported the sensitivity and limit of detection (LOD). The proposed numerical methods show much higher sensitivity and lower detection limits than the traditional techniques. The observed detection limits are as low as ~2 × 10^{-6} refractive index unit changes near the surface. The proposed methods can be utilized for any sensing systems that employ transmission spectra and will outperform traditional methods if there are multiple peaks present in the transmission spectra.**

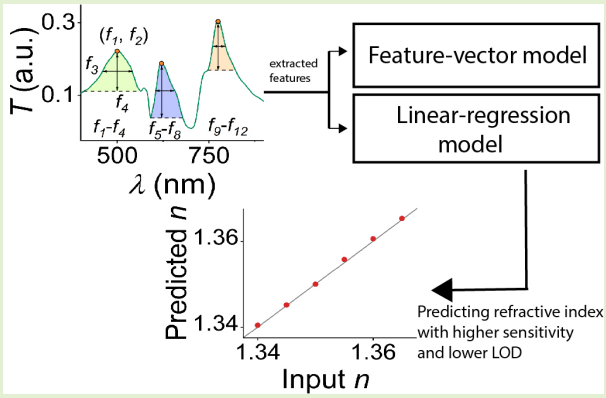

***Index Terms*— Biosensors, limit of detection (LOD), plasmonics.**

I. Introduction

PLASMONICS—THE study of generation, detection, and manipulation of electromagnetic waves at the metal–dielectric interface—has gained significant attention over the past few decades because of its vast applications in sensing, communication, and biophotonics [1], [2], [3]. Plasmonics utilizes a phenomenon called surface plasmon resonance (SPR), the resonant oscillation of free electrons at the metal–dielectric interface due to the interaction with the incident light [4]. SPR modes are strongly confined at the metal–dielectric interface and highly sensitive to small refractive index changes near the interface. Therefore, SPR has been extensively applied in biosensing, gas and chemical sensing, and molecular binding analysis [5], [6], [7].

Manuscript received 21 February 2023; revised 14 April 2023; accepted 14 April 2023. Date of publication 1 May 2023; date of current version 14 June 2023. The associate editor coordinating the review of this article and approving it for publication was Dr. Rui Min. *(Tashfiq Ahmed and A. K. M. Naziul Haque contributed equally to this work.) (Corresponding author: Muhammad Anisuzzaman Talukder.)*

Tashfiq Ahmed and Muhammad Anisuzzaman Talukder are with the Electrical and Electronic Engineering, Bangladesh University of Engineering and Technology, Dhaka 1205, Bangladesh (e-mail: tashfiq@eee.buet.ac.bd; anis@eee.buet.ac.bd).

A. K. M. Naziul Haque is with the Computer Science and Engineering, Brac University, Dhaka 1212, Bangladesh (e-mail: naziul.haque@bracu.ac.bd).

Digital Object Identifier 10.1109/JSEN.2023.3270439

Usually, SPR is achieved using a bulky prism, for example, in the Kretschmann configuration, and diffraction grating [6], [8], [9], [10]. These configurations often require considerable space and incidence angle-sensitive setups, limiting multiplexing density, high-throughput biosensing, and integration with lab-on-chip (LOC). In addition, these SPR sensors require complex arrangements for detecting single or small biological and chemical interactions, and hence, challenging to deploy in resource-poor and compact settings.

The localized SPR (LSPR) phenomenon [11], [12] and extraordinary transmission (EOT) through subwavelength metallic periodic nanoaperture [10], [13], [14], [15] have recently gained significant attention to improve the limit of detection (LOD) and increase the throughput of sensors. Strong field confinement resulting from LSPR and noticeable change in the EOT characteristics with minute changes in the local refractive index allows better sensing performance. Plasmonic biosensors with subwavelength nanoaperture, particularly periodic nanohole arrays on metallic films, exhibit strong light confinement and field enhancement at the dielectric–metal interface. The characteristics of the confined light sensitively depend on the slight refractive index changes near the surface, leading to the development of sensitive refractive index sensors capable of detecting small quantities of bioanalytes [16], [17], [18], [19], [20], [21], [22], [23], [24],

[25]. Nanohole array-based biosensors have several advantages: ultrasensitive, label-free real-time detection-capable, compact, simple, cheap, and lightweight [26], [27], [28], [29]. Furthermore, multiple arrays can be incorporated with complex fluidic structures for multiple and parallel analyte sampling and detection, as in an LOC-sensing device [16], [25], [29].

In periodic nanohole array structures, multiple peaks occur at the transmission spectra because of the SPR and grating coupling conditions. It has been reported that by using these multiple peaks and applying the spectral integration method, higher sensitivity and lower LOD can be achieved compared to the single peak-shift method [14], [30]. It has also been reported that the sensitivity can be enhanced further by optimizing structural parameters, such as nanohole diameter, periodicity, and shape [31]. However, achieving a detection limit comparable to traditional highly-sensitive bulky SPR sensors is still challenging for these nanohole array-based biosensors.

In this work, we propose two numerical techniques utilizing features of multiple peaks in the transmission spectra of a gold (Au) nanohole array for higher sensitivity and lower LOD. First, we focus on the benefits of using multiple transmission peak features rather than a single peak shift. We then introduce our proposed numerical techniques: Feature vector and multiple linear regression models. We present the optimized structural parameters of the gold nanohole array for improved biosensing performance using the proposed numerical techniques. We have calculated the biosensor sensitivity using the proposed techniques in the presence of noise. We have also determined the LOD and compared it with traditional methods. Lastly, we have simulated two real-life critical biosensing applications and reported the sensor performance using the proposed numerical techniques.

II. Nanohole Structure and Sensitivity Using Single and Multiple Resonances

This work uses a symmetric periodic gold nanohole array structure for the sensor, as shown in Fig. 1(a). The sensor structure resembles that experimentally reported in [32]. Initially, we set the nanohole diameter (d), periodicity (P), and the Au metal layer thickness (t) to 150, 400, and 50 nm, respectively. The top sample material and bottom glass layer thicknesses are set to 800 nm. We set perfectly matched layer boundary conditions at the top and bottom and periodic boundary conditions at the other boundaries. We simulated a unit cell of the structure, as shown in Fig. 1(a), for transverse magnetic (TM)-polarized incident light using the finite-difference time-domain (FDTD) numerical technique. Because of the dependence of plasmonic excitation on grating coupling conditions, maxima in the EOT spectra occur at wavelengths given by [31], [33]

$$\lambda_{SP} = \sqrt{\frac{\epsilon_d \epsilon_m}{\epsilon_d + \epsilon_m}} \frac{P}{\sqrt{i^2 + j^2}}. \tag{1}$$

Here, P is the array periodicity, integers i and j are the Bragg resonance orders, and ϵ_d and ϵ_m are the dielectric constants of dielectric material and metal, respectively. The performed FDTD simulations in this work exhibit EOT characteristics with multiple resonance peaks, as shown in Fig. 1(b). One significant benefit of the gold nanohole biosensor is the presence of multiple resonance peaks in the transmission spectra that can be used for higher sensitivity. The transmission spectra of the gold nanohole array are highly sensitive to surface refractive index changes due to intense field enhancement near the surface of the nanoholes resulting from plasmonic resonance. Therefore, a small refractive index change near the surface results in a detectable change in the EOT characteristics. Thus, the plasmon resonances and EOT improve the sensor's detection limit.

First, we calculate the sensitivity of traditional peak shift and spectral integration methods to demonstrate the advantages of using multiple peaks over a single peak for sensing tiny changes in the sample refractive index. We considered the transmission spectra as the reference when the sample material has a refractive index of 1.33 (water). To calculate the sensing performance of biosensors, we have varied the sample material's refractive index, n, from 1.340 to 1.365, representing different concentrations (v/v) of glycerin solution [34]. After analyzing the transmission spectra, as shown in Fig. 1(b), we have found that the third peak at 780 nm is the most sensitive as the peak position varies the most with the refractive index. For example, this peak varies from 773 to 783 nm as the refractive index varies from 1.34 to 1.3675. On the other hand, the first and the second peaks vary only by 2 and 3 nm, respectively, for the same refractive index change. In addition, all the features related to the third peak are more sensitive to refractive index changes. Therefore, we calculated the wavelength shift of the most sensitive third peak. A linear relationship exists between the peak shift and sample refractive index, as shown in Fig. 1(c). For the peak-shift method, the sensor sensitivity S_λ is defined as the slope of the peak position versus the sample material's refractive index curve given by

$$S_\lambda = \frac{\partial \lambda_R}{\partial n}. \tag{2}$$

Here, λ_R represents the peak position. The calculated sensitivity is 275 nm/RIU.

The spectral integration method has been applied for nanostructured sensors, especially nanohole array biosensors. Compared to the traditional peak-shift method, the critical advantage of this integral method is the utilization of the entire transmission spectra for sensing rather than just a single peak value. The spectral integration method has resulted in higher sensitivity, lower LOD, and better sensing performance [14], [25], [30], [34], [35]. We employed the spectral integration method to calculate the sensor sensitivity. Spectral integral value $R(n)$ and sensitivity S_R are defined as

$$R(n) = \sum_{\lambda_1}^{\lambda_2} \left| \frac{T(n,\lambda) - T(n_0,\lambda)}{T(n_0,\lambda)} \right| \times \Delta\lambda \tag{3a}$$

$$S_R = \frac{\partial R}{\partial n}. \tag{3b}$$

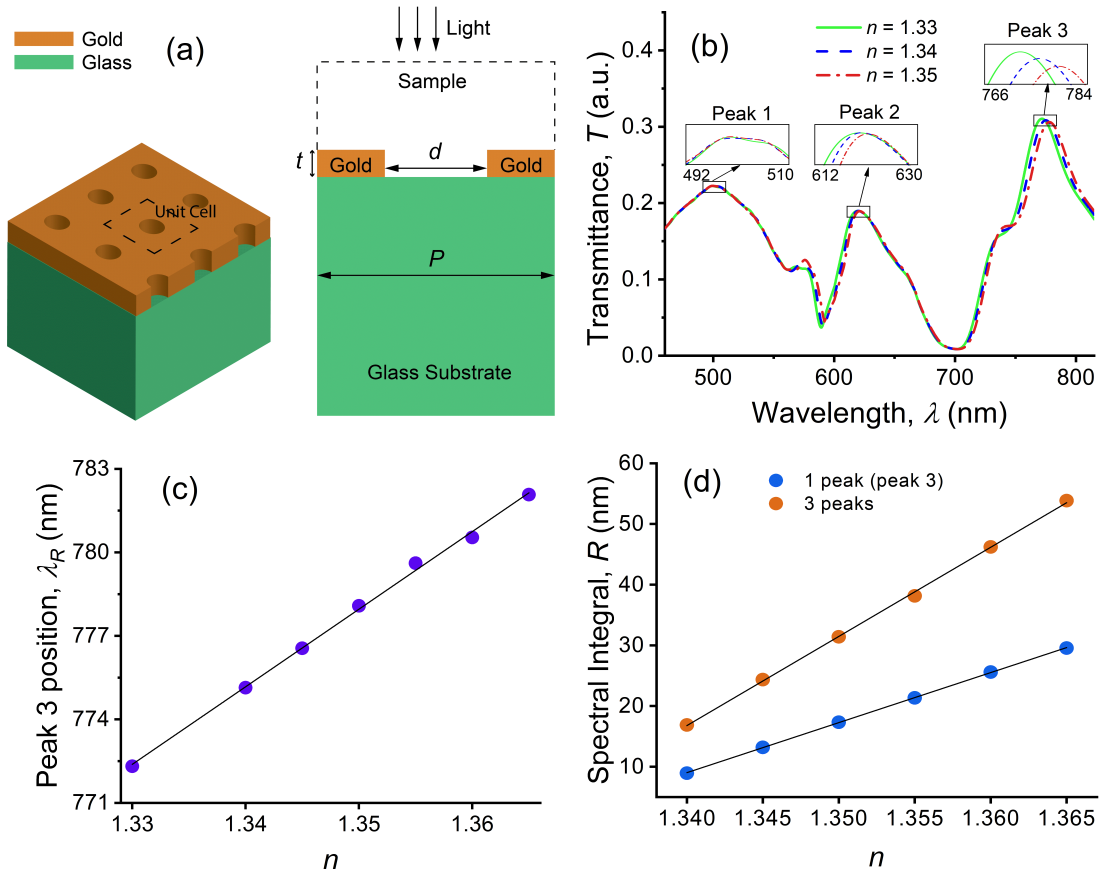

Fig. 1. (a) Gold nanohole biosensor structure, showing various structural parameters. Here, the array periodicity, $P = 400$ nm, nanohole diameter, $d = 150$ nm, and gold layer thickness, $t = 50$ nm. (b) Transmission spectra, (c) peak 3 position, which is the most sensitive peak (sensitivity, $S_\lambda = 278$ nm/RIU), and (d) spectral integral value for only peak 3 (sensitivity, $S_{R1} = 824$ nm/RIU) and all peaks (sensitivity, $S_{R3} = 1468$ nm/RIU) for different sample refractive indices.

Here, $T(n_0, \lambda)$ stands for reference transmittance values [14], [30].

To illustrate the benefits of using multiple peaks for sensing, we have compared spectral integral values and sensitivities for two cases: considering 1) only the spectral region near the most sensitive peak and 2) the entire transmission spectra encompassing all peaks within the wavelength range of 450–900 nm [34]. The transmission spectra for the refractive index of 1.33 (water) are considered as the reference, and we varied the sample refractive index from 1.340 to 1.365. For both cases, a linear relationship exists between the spectral integral value and the sample refractive index, as shown in Fig. 1(d). We notice higher sensitivity if multiple peaks are considered compared to the sensitivity obtained from the single peak region. Our calculated sensitivities considering the single peak region and the entire spectra are 824 and 1469 nm/RIU, which are higher than the peak-shift method. Therefore, higher sensitivity can be achieved using multiple peaks and the traditional spectral integration method compared to the single peak shift method.

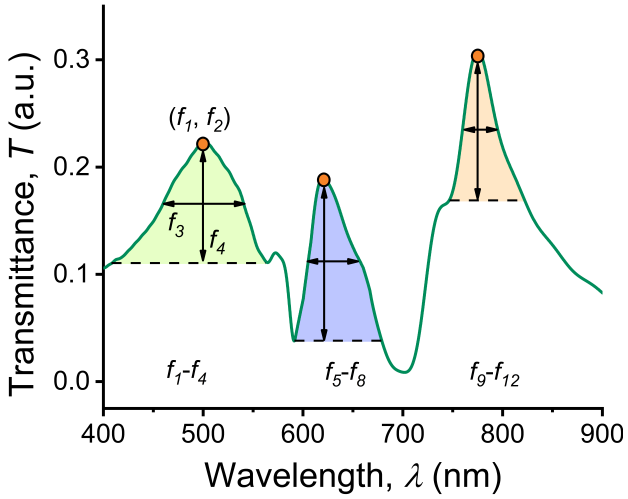

Fig. 2. Transmission spectra of the gold nanohole array, identifying peaks and features.

III. Numerical Methods Utilizing Multiple Features

This section demonstrates how features extracted from multiple peaks can enhance the sensor performance further and proposes two numerical methods: the feature vector model and the linear regression model. In our approaches, we consider multiple transmission resonances' peak position, intensity, linewidth, and prominence as feature variables. The peak prominence indicates how much a particular peak

stands out relative to the surrounding peaks. Fig. 2 shows the transmission spectra of the gold nanohole array structure. The transmission spectra have three resonance peaks. We extracted four features from each peak, that is, position, intensity, linewidth, and prominence, totaling 12 features from the transmission spectra. The relationships of these 12 features (f_1–f_{12}) with the refractive index are presented in Fig. 3. After analyzing these features, we found that each feature exhibits a different relationship with the sample refractive index. We note that not all of these 12 features linearly depend on the sample refractive index. The feature values (f_i) extracted from the transmission spectra for sample refractive index $n = 1.34$ are listed in Table I. In Sections III-A and III-B, we elucidate how these multiple features can be used in our proposed numerical methods to enhance sensing capability.

A. Feature Vector Model

Now, we propose a feature vector model that employs features extracted from multiple transmission peaks to enhance biosensing capabilities. The motivation behind proposing this model is to take advantage of the information from the multiple peaks of the transmission spectra to achieve greater sensitivity and lower detection limits from a sensor. In the typical peak-shift method, we record only the center wavelength of the most sensitive peak of the transmission spectra with the sample material's refractive index. The sensitivity is then determined using (2). The "feature vector model" extends the peak-shift method by employing a "feature vector" instead of a single feature, for example, peak wavelength, for calculating the sensitivity and LOD. The feature vector, $\mathbf{V_f}(n)$, contains multiple features obtained from different peaks and can be written as

$$\mathbf{V_f}(n) = \begin{bmatrix} f_1 \\ f_2 \\ \vdots \\ f_i \end{bmatrix}. \tag{4}$$

The proposed feature vector method generalizes the peak-shift method and outperforms it in sensitivity and LOD, as detailed later in this subsection. We now define sensitivity, S_f, for the feature vector method. To do this, we first quantify the change in feature vector in higher-dimensional space due to the change in the sample material's refractive index using the Euclidean distance, D, given by

$$D(n) = ||\mathbf{V_f}(n) - \mathbf{V_f}(n_0)|| \tag{5}$$

where $\mathbf{V_f}(n_0)$ is the feature vector obtained for the reference refractive index. Then, the sensitivity is, like the peak-shift and spectral integration methods, the slope of the distance versus sample refractive index curve written as

$$S_f = \frac{\partial D}{\partial n}. \tag{6}$$

The experimentally obtained sensitivity and LOD results may deviate from the ideal case due to shot noise, environmental effects, and sample defects. These effects might significantly limit the sensitivity and LOD of biosensors. The detection limit increases with noise power, and the biosensor performance deteriorates. Therefore, we must incorporate the effects of noise in our simulation to simulate a realistic case. For optical biosensors, a noise signal with a signal-to-noise ratio (SNR) of 60 dB can be used to model a realistic case [36], [37].

We added additive white Gaussian noise (AWGN) to the transmission spectra to calculate the LOD, keeping the SNR at 60 dB. We followed the LOD calculation approach discussed in [36]. The added noise makes it challenging to identify the transmission peaks accurately. Therefore, we first applied a Gaussian weighted moving average filter with a 2-nm window to smooth the transmission spectra and identify the peaks accurately. Then, we determined features from regions surrounding each transmission peak. We performed min-max normalization to the feature vector as the features have different units and ranges. Furthermore, we have chosen only those features that individually show a linear relationship with the sample refractive index, for example, f_{10}, as shown in Fig. 3, ensuring that the feature vector containing these selected features has a distance function $D(n)$ that varies almost linearly with the refractive index. The distance versus the sample refractive index is shown in Fig. 4(a) with a reference index n_0 of 1.340 and a feature vector with seven features.

The peak-shift method can be viewed as a special case of the feature vector method when the feature vector contains only the peak wavelength as the feature. For this 1-D feature vector, (5) and (6) produce the same sensitivity as the peak-shift method. However, higher sensitivity can be achieved by incorporating more features. When we use more than one feature, the distance function $D(n)$ becomes greater than the distance function obtained for a single feature. To explain this, let us assume that $D_i(n)$ is the distance function obtained for a feature vector $V_i(n)$ with i features. Then, we add one more feature to $V_i(n)$ to obtain the feature vector $V_{i+1}(n)$ and distance function $D_{i+1}(n)$. Now, from the definition, $D_i(n)$ and $D_{i+1}(n)$ can be written as

$$D_i(n) = \sqrt{(\Delta f_1)^2 + \cdots + (\Delta f_i)^2} \tag{7a}$$

$$D_{i+1}(n) = \sqrt{(\Delta f_1)^2 + \cdots + (\Delta f_i)^2 + (\Delta f_{i+1})^2}. \tag{7b}$$

Therefore, $D_i(n) \leq D_{i+1}(n)$, if the $(i+1)$th feature varies linearly with the sample refractive index. Moreover, this inequality ensures that $D_{i+1}(n)$ will have a higher slope than $D_i(n)$, because $D_i(n) = D_{i+1}(n) = 0$ for $n = n_0$ and $D_{i+1}(n) > D_i(n)$ for $n > n_0$. As a result, according to (6), we will obtain higher sensitivity by using additional features. However, for these statements to be valid, the individual features of the feature vector must have a linear relation with the sample refractive index.

Similar to sensitivity improvement, using multiple features increases detection capability, as LOD is inversely related to sensitivity [36]. To calculate the overall LOD of the sensor, we calculated the minimum detectable change in the presence of 60 dB AWG noise for refractive indices ranging from 1.34 to 1.3675. For a specific refractive index, LOD is calculated using three times the standard deviation from

TABLE I
FEATURE VALUES FROM THREE TRANSMISSION SPECTRA PEAKS WHEN $n = 1.34$

Feature	Value	Feature	Value	Feature	Value
f_1	499.588 (nm)	f_5	620.084 (nm)	f_9	775.038 (nm)
f_2	0.222 (a.u.)	f_6	0.1897 (a.u.)	f_{10}	0.3084 (a.u.)
f_3	53.32 (nm)	f_7	33.85 (nm)	f_{11}	36.44 (nm)
f_4	0.116 (a.u.)	f_8	0.1518 (a.u.)	f_{12}	0.226 (a.u.)

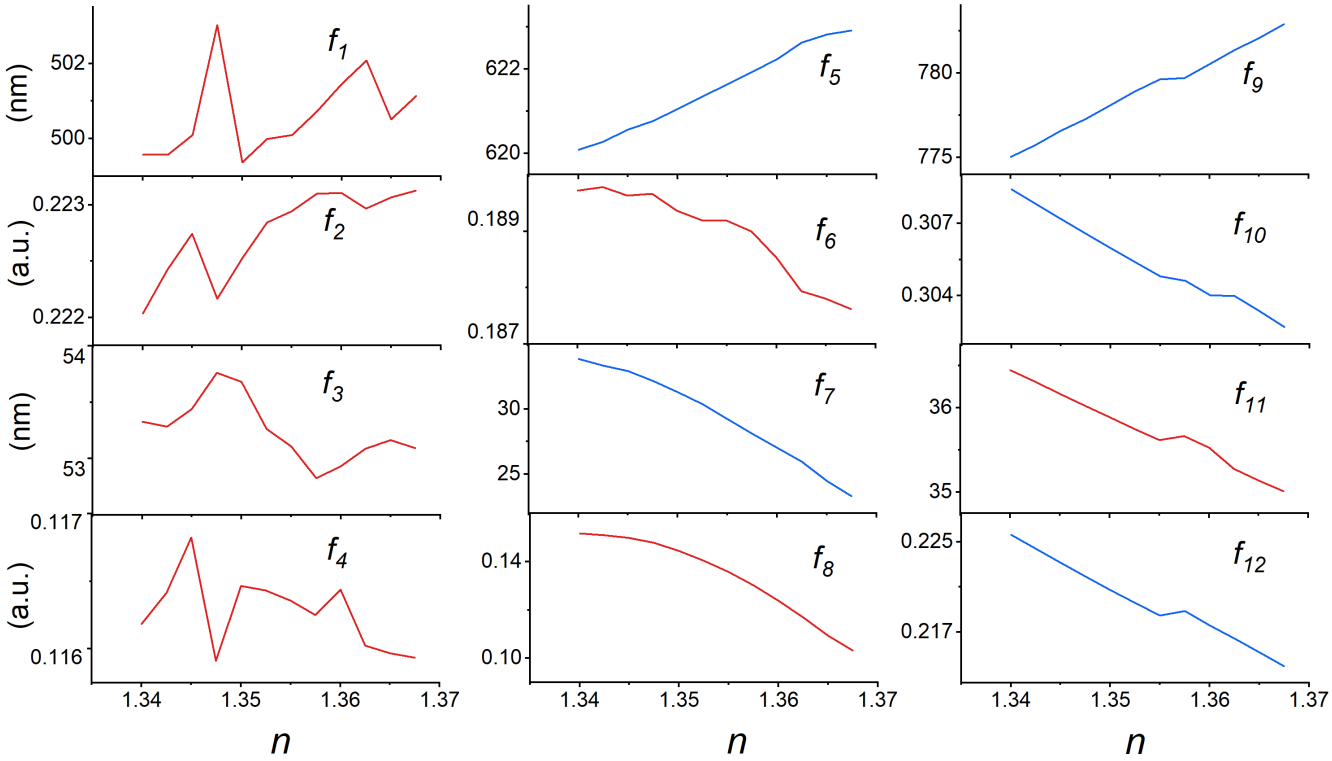

Fig. 3. Relationships of the features f_1–f_{12} with the sample refractive index.

the mean value. After calculating LODs for refractive indices ranging from 1.34 to 1.3675 with a step size of 0.0025, we calculated the mean LOD for this refractive index range. This average LOD is then used as a performance parameter for the proposed models [25]. Fig. 4(b) demonstrates that LOD significantly decreases as more features are used. Using seven features, we got an LOD value of one-fifth of the LOD value obtained with a single feature. Therefore, by introducing a multidimensional feature vector, we could extend the traditional peak-shift method and significantly improve the detection limit.

B. Linear Regression Model

We propose a multiple linear regression model to achieve even higher sensitivity using the features of multiple peaks. We varied the sample refractive index on top of the structure from 1.340 to 1.3675 with a step of 0.0025. We calculated the transmission spectra and identified the resonance peaks. We then extracted features from the three resonance peaks, as discussed before. As shown in Fig. 3, not all these features linearly vary with the sample refractive index. Therefore, we eliminated the redundant nonlinear features from our linear regression model. For specific structural parameters, such as nanohole diameter, periodicity, and metal thickness, we found that five features, that is, f_5, f_7, f_9, f_{10}, and f_{12}, exhibit best linear relationships with the sample refractive index. Furthermore, the ranges of different feature values are quite different, as tabulated in Table I. Hence, we scaled the features so that the ranges are similar and the regression model performs better. The sample refractive index using the regression model can be expressed as

$$n = \beta_0 + \beta_1 f_1' + \beta_2 f_2' + \cdots + \beta_j f_j' + \cdots + \beta_p f_p' + \epsilon \quad (8)$$

where f_j' is the scaled linear feature, β_0 is the constant y-intercept, β_j is the slope coefficient for the jth feature, p is the total number of features used in the model, and ϵ is the error, also known as the residual.

We trained our multiple linear regression model using the transmission data and known refractive indices using (8). Thus, we found the β_j coefficients to result in the best-fit relationship with the minimum mean squared error. Finally, we can predict any refractive index from the transmission data and use the obtained model.

We again added an AWGN with 60-dB SNR to the simulated transmission spectra to determine the effects of noise on the linear regression model's performance and LOD.

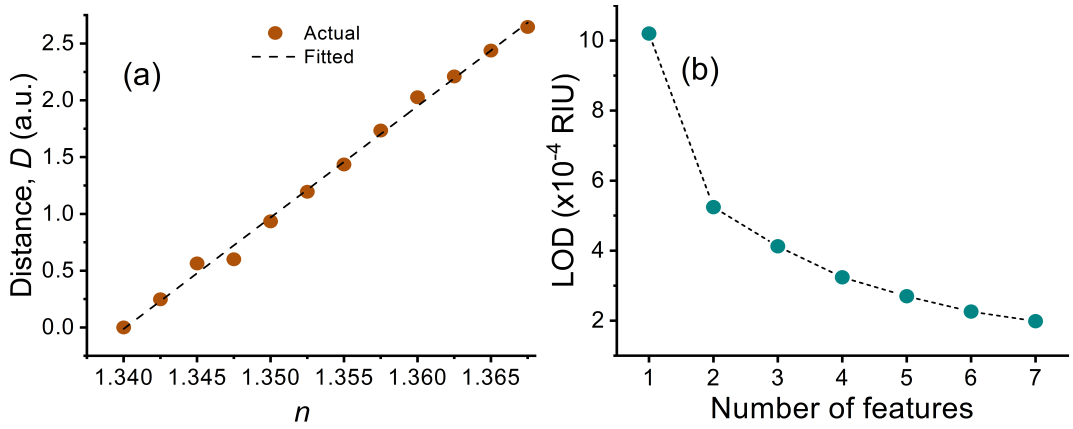

Fig. 4. (a) Distance function (D) of the feature vector model against the sample refractive index (n) using feature vector model (sensitivity, $S_f = 98$ a.u./RIU) and (b) LOD versus number of features.

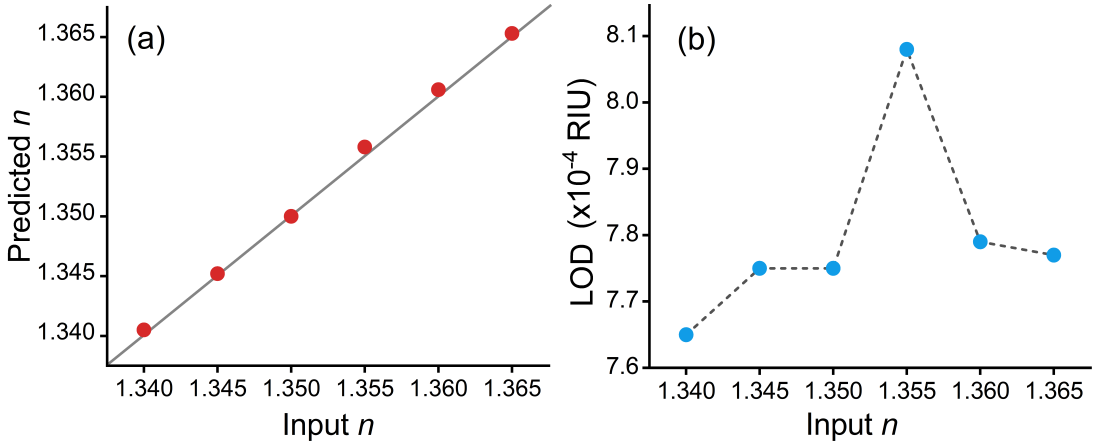

Fig. 5. (a) Predicted sample refractive index versus actual sample refractive index using the linear regression model. The gray straight line has a unit slope. (b) LOD versus actual sample refractive index.

Fig. 5 shows the linear regression model's performance in predicting the sample refractive index and LOD for different sample refractive indices. The predicted n closely matches the sample n, as shown in Fig. 4(a). The calculated LOD remains $<8.1 \times 10^{-4}$ RIU for different sample refractive indices, with an average LOD of 7.8×10^{-4} RIU, as shown in Fig. 4(b).

IV. Optimized Structure Performance

We further tuned structural parameters such as nanohole diameter, periodicity, and metal thickness in the quest for higher sensitivity and lower LOD. We applied the grid search method for optimizing the structural parameters to achieve the lowest LOD. We varied the nanohole diameter, array periodicity, and metal layer thickness while searching for the lowest LOD. Using this method, we found a nanohole diameter, periodicity, and metal thickness of 150, 600, and 150 nm, respectively, that resulted in the lowest LOD.

We considered the issues related to the practical realization of the proposed metasurface and the structure. The proposed metasurface and structure are realizable using the available standard fabrication technologies. To date, several techniques have been reported for the fabrication of metallic nanohole structures and metasurfaces [38]. For example, focused ion beam (FIB) milling and electron-beam lithography (EBL) techniques have been employed for nanohole array fabrication. In EBL, a photoresist coating is applied to the substrate, and then the structure is exposed to an electron beam, followed by chemical development. Then Au layer is deposited on top using metal deposition techniques, and usually, a thin layer of Cr deposition follows the Au deposition. Recently, a lift-off free nanofabrication scheme has attracted significant interest [25]. Several other techniques, such as template stripping and soft interface lithography, have also been introduced. The structural parameters of the proposed structures are well within the current capability of the fabrication techniques [39].

Once again, we varied sample refractive indices, calculated the transmission spectra, and further examined the effect of noise by introducing noise to the transmission spectra so that the SNR is 60 dB. We calculated features from the smoothed transmission spectra. Next, we compare the performance of the feature vector and linear regression models for the optimized structure. Fig. 6(a) and (b) shows the predicted n and LOD for the feature vector and linear regression models. The regression model predicts the sample refractive index better than the feature vector model. Moreover, the regression model's variance is also smaller, as demonstrated by the lower LOD. However, the feature vector model can be advantageous in situations when more linear features are available. In the feature vector model, the performance enhances as more features are included in the model.

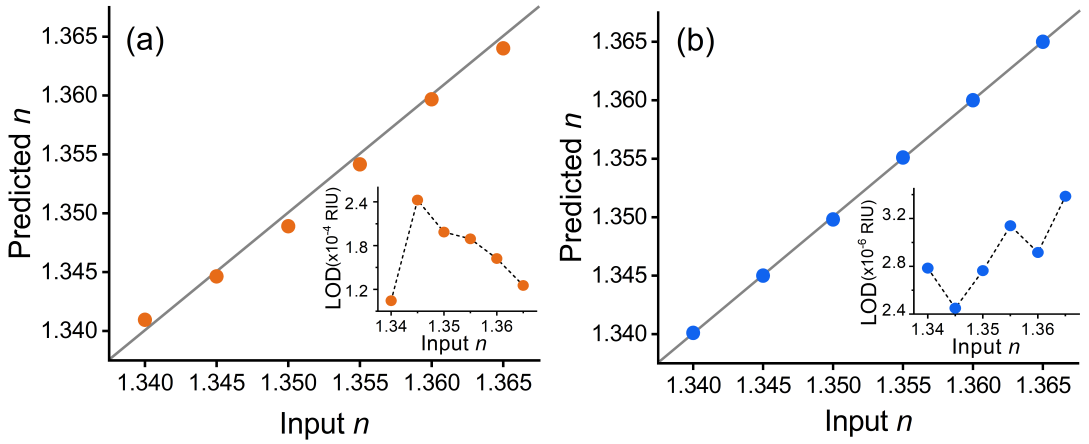

Fig. 6. Predicted refractive index versus input value for optimized structures using (a) feature vector model and (b) linear regression model. Insets show LODs for 60-dB SNR. In both cases, the gray straight line has a unit slope.

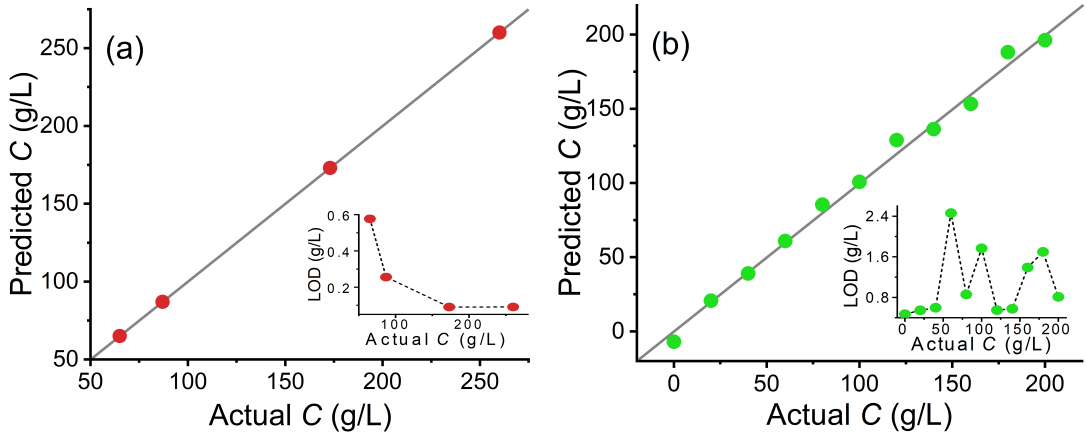

Fig. 7. Predicted concentration versus actual concentration for (a) hemoglobin and (b) glucose solution using optimized structural parameters and linear regression model. Insets show LOD for noise added to the transmission spectra with 60-dB SNR. In both cases, the gray straight line has a unit slope.

In contrast, our study has not observed such monotonic behavior of the LOD curve against the feature number for the linear regression model. The lowest calculated LODs for the linear regression and feature vector models are 2.45×10^{-6} RIU and 1.99×10^{-4} RIU, respectively. The calculated LOD is much smaller than the reported LODs for both the peak-shift and spectral integration methods [25], [40], [41], [42], [43], [44], [45]. The average LOD for the optimized structure using traditional peak shift and spectral integration methods is compared with the proposed feature vector and linear regression models in Table II. The proposed feature vector model, an extension of the peak-shift method, exhibits a much lower LOD than the peak-shift method. The linear regression model demonstrates a much lower LOD than both traditional methods. Thus, using the optimized structure, the LOD of the sensor has been significantly improved.

TABLE II
COMPARISON OF THE OBTAINED LOD USING DIFFERENT NUMERICAL MODELS FOR OUR OPTIMIZED STRUCTURE

Model	LOD ($\times 10^{-6}$ RIU)
Peak-shift	1020
Spectral Integration	148
Feature Vector	199
Linear Regression	2.45

V. APPLICATIONS IN BIOSENSING

We applied the proposed models in two biosensing applications, such as determining hemoglobin and glucose concentrations in blood. Hemoglobin is a protein responsible for the transportation of oxygen and carbon dioxide. Therefore, patients need to monitor and maintain proper hemoglobin levels in the blood. It has been well reported that the refractive index of hemoglobin changes significantly with its concentration [46]. We used hemoglobin refractive indices versus its concentrations from 0 to 260 g/L from the literature [46]. The refractive indices are also considered dispersive. First, using the feature vector model, we calculated the sensitivity and then used it to evaluate LOD. The calculated sensitivity and LOD values are 0.018 a.u./gL^{-1} and 1.1 g/L, respectively. Next, using the proposed linear regression model and the discussed methodology, we predicted the hemoglobin concentration from simulated transmission spectra under the effect of noise. The predicted and actual concentrations

are shown in Fig. 7(a). The average LOD achieved is 0.254 g/L. The numerical technique's prediction performance greatly depends on the number of sample data. Only limited experimental refractive index versus concentration data are available, affecting the prediction performance of the technique.

Second, we simulated an aqueous solution with different glucose concentrations. Like the case of hemoglobin, the refractive index varies with the glucose concentration. We used experimentally reported refractive index of different glucose concentrations [47]. It has been reported that a linear relationship exists between the refractive index and the glucose concentration [47]. The solution's refractive index changes from 1.33128 to 1.35497 for glucose concentrations of zero to 200 g/L. For the feature vector model, the calculated sensitivity and LOD values are 0.012 a.u./gL^{-1} and 1.68 g/L, respectively. In addition, the linear regression model results are shown in Fig. 7(b). The LOD varies from 0.427 to 2.4616 g/L in the presence of noise, with an average LOD of 1.1 g/L.

VI. Conclusion

In conclusion, we have proposed two numerical methods—feature vector and linear regression models—to utilize features from multiple transmission peaks and achieve higher sensitivity and lower LOD than traditional techniques from gold nanohole array-based biosensors. The proposed models use features that vary linearly with the sample refractive index changes. The predicted sample refractive index and LOD have been calculated in the presence of AWGN with 60 dB SNR and a smoothing filter to consider a realistic system. The proposed linear regression model performs better than the feature vector model, resulting in an LOD as low as 2.45×10^{-6} RIU from the optimized gold nanohole array-based sensor structure. The proposed techniques have been demonstrated to detect ultralow hemoglobin and glucose concentrations with high accuracy. Our proposed methods consider multiple features from transmission peaks and utilize the additional information to lower LOD and increase the sensor's sensitivity. Traditionally, the peak-shift method uses only the change in a single peak for sensing, and the spectral integration method includes only the percentage change in the transmission spectra. In contrast, our proposed approaches improve sensor performances by including more relevant features. The proposed methods can be used for other sensing systems and will produce better results than traditional methods if multiple resonance peaks are available in the transmission spectra.

References

[1] L. Novotny and B. Hecht, *Principles of Nano-Optics*. Cambridge, U.K.: Cambridge Univ. Press, 2012.

[2] S. A. Maier, M. L. Brongersma, P. G. Kik, S. Meltzer, A. A. G. Requicha, and H. A. Atwater, "Plasmonics—A route to nanoscale optical devices," *Adv. Mater.*, vol. 13, no. 19, pp. 1501–1505, Sep. 2001.

[3] D. K. Gramotnev and S. I. Bozhevolnyi, "Plasmonics beyond the diffraction limit," *Nature Photon.*, vol. 4, no. 2, pp. 83–91, 2010.

[4] S. Zeng, D. Baillargeat, H. P. Ho, and K. T. Yong, "Nanomaterials enhanced surface plasmon resonance for biological and chemical sensing applications," *Chem. Soc. Rev.*, vol. 43, no. 10, pp. 3426–3452, Apr. 2014.

[5] R. T. Hill, "Plasmonic biosensors," *Wiley Interdiscipl. Rev., Nanomed. Nanobiotechnol.*, vol. 7, no. 2, pp. 152–168, 2015.

[6] J. Homola, "Surface plasmon resonance sensors for detection of chemical and biological species," *Chem. Rev.*, vol. 108, no. 2, pp. 462–493, 2008.

[7] S. Roh, T. Chung, and B. Lee, "Overview of plasmonic sensors and their design methods," *Proc. SPIE*, vol. 7853, Jan. 2010, Art. no. 785303.

[8] C. Nylander, B. Liedberg, and T. Lind, "Gas detection by means of surface plasmon resonance," *Sens. Actuators*, vol. 3, pp. 79–88, Jan. 1982.

[9] I. Richter, P.-C. Sun, F. Xu, and Y. Fainman, "Design considerations of form birefringent microstructures," *Appl. Opt.*, vol. 34, no. 14, pp. 2421–2429, 1995.

[10] K. A. Tetz, L. Pang, and Y. Fainman, "High-resolution surface plasmon resonance sensor based on linewidth-optimized nanohole array transmittance," *Opt. Lett.*, vol. 31, no. 10, pp. 1528–1530, May 2006.

[11] P. Hanarp, M. Käll, and D. S. Sutherland, "Optical properties of short range ordered arrays of nanometer gold disks prepared by colloidal lithography," *J. Phys. Chem. B*, vol. 107, no. 24, pp. 5768–5772, Jun. 2003.

[12] T. Rindzevicius, Y. Alaverdyan, A. Dahlin, F. Höök, D. S. Sutherland, and M. Käll, "Plasmonic sensing characteristics of single nanometric holes," *Nano Lett.*, vol. 5, no. 11, pp. 2335–2339, Nov. 2005.

[13] A. G. Brolo, R. Gordon, B. Leathem, and K. L. Kavanagh, "Surface plasmon sensor based on the enhanced light transmission through arrays of nanoholes in gold films," *Langmuir*, vol. 20, no. 12, pp. 4813–4815, Jun. 2004.

[14] M. E. Stewart et al., "Quantitative multispectral biosensing and 1D imaging using quasi-3D plasmonic crystals," *Proc. Nat. Acad. Sci. USA*, vol. 103, no. 6, pp. 17143–17148, 2006.

[15] A. De Leebeeck, L. K. S. Kumar, V. de Lange, D. Sinton, R. Gordon, and A. G. Brolo, "On-chip surface-based detection with nanohole arrays," *Anal. Chem.*, vol. 79, no. 11, pp. 4094–4100, Jun. 2007.

[16] A. A. Yanik et al., "An optofluidic nanoplasmonic biosensor for direct detection of live viruses from biological media," *Nano Lett.*, vol. 10, no. 12, pp. 4962–4969, Dec. 2010.

[17] A. A. Yanik et al., "Seeing protein monolayers with naked eye through plasmonic Fano resonances," *Proc. Nat. Acad. Sci. USA*, vol. 108, no. 29, pp. 11784–11789, Jul. 2011.

[18] A. A. Yanik, M. Huang, A. Artar, T.-Y. Chang, and H. Altug, "Integrated nanoplasmonic-nanofluidic biosensors with targeted delivery of analytes," *Appl. Phys. Lett.*, vol. 96, no. 2, Jan. 2010, Art. no. 021101.

[19] A. Artar, A. A. Yanik, and H. Altug, "Fabry–Pérot nanocavities in multilayered plasmonic crystals for enhanced biosensing," *Appl. Phys. Lett.*, vol. 95, no. 5, 2009, Art. no. 051105.

[20] F. Eftekhari, R. Gordon, J. Ferreira, A. G. Brolo, and D. Sinton, "Polarization-dependent sensing of a self-assembled monolayer using biaxial nanohole arrays," *Appl. Phys. Lett.*, vol. 92, no. 25, Jun. 2008, Art. no. 253103.

[21] M. Huang, B. C. Galarreta, A. E. Cetin, and H. Altug, "Actively transporting virus like analytes with optofluidics for rapid and ultrasensitive biodetection," *Lab Chip*, vol. 13, no. 24, pp. 4841–4847, 2013.

[22] A. Blanchard-Dionne, L. Guyot, S. Patskovsky, R. Gordon, and M. Meunier, "Intensity based surface plasmon resonance sensor using a nanohole rectangular array," *Opt. Exp.*, vol. 19, no. 16, pp. 15041–15046, 2011.

[23] H. Gao, J. Henzie, and T. W. Odom, "Direct evidence for surface plasmon-mediated enhanced light transmission through metallic nanohole arrays," *Nano Lett.*, vol. 6, no. 9, pp. 2104–2108, Sep. 2006.

[24] G. C. Schatz, J. M. McMahon, and S. K. Gray, "Tailoring the parameters of nanohole arrays in gold films for sensing applications," *Proc. SPIE*, vol. 6641, Sep. 2007, Art. no. 664103.

[25] A. E. Cetin and H. Altug, "Fano resonant ring/disk plasmonic nanocavities on conducting substrates for advanced biosensing," *ACS Nano*, vol. 6, no. 11, pp. 9989–9995, Nov. 2012.

[26] N. Liu, M. L. Tang, M. Hentschel, H. Giessen, and A. P. Alivisatos, "Nanoantenna-enhanced gas sensing in a single tailored nanofocus," *Nature Mater.*, vol. 10, no. 8, pp. 631–636, Aug. 2011.

[27] F. Mazzotta, T. W. Johnson, A. B. Dahlin, J. Shaver, S.-H. Oh, and F. Höök, "Influence of the evanescent field decay length on the sensitivity of plasmonic nanodisks and nanoholes," *ACS Photon.*, vol. 2, no. 2, pp. 256–262, Feb. 2015.

[28] A. E. Cetin et al., "Handheld high-throughput plasmonic biosensor using computational on-chip imaging," *Light, Sci. Appl.*, vol. 3, no. 1, p. e122, Jan. 2014.
[29] A. F. Coskun, A. E. Cetin, B. C. Galarreta, D. A. Alvarez, H. Altug, and A. Ozcan, "Lensfree optofluidic plasmonic sensor for real-time and label-free monitoring of molecular binding events over a wide field-of-view," *Sci. Rep.*, vol. 4, no. 1, pp. 1–7, Oct. 2014.
[30] K.-L. Lee and P.-K. Wei, "Enhancing surface plasmon detection using ultrasmall nanoslits and a multispectral integration method," *Small*, vol. 6, no. 17, pp. 1900–1907, Sep. 2010.
[31] A. Prasad, J. Choi, Z. Jia, S. Park, and M. R. Gartia, "Nanohole array plasmonic biosensors: Emerging point-of-care applications," *Biosensors Bioelectron.*, vol. 130, pp. 185–203, Apr. 2019.
[32] L. Wu, P. Bai, X. Zhou, and E. P. Li, "Reflection and transmission modes in nanohole-array-based plasmonic sensors," *IEEE Photon. J.*, vol. 4, no. 1, pp. 26–33, Feb. 2012.
[33] T. W. Ebbesen, H. J. Lezec, H. F. Ghaemi, T. Thio, and P. A. Wolf, "Extraordinary optical transmission through sub-wavelength hole arrays," *Nature*, vol. 391, pp. 667–669, Feb. 1998.
[34] E.-H. Lin, W.-S. Tsai, K.-L. Lee, M.-C. M. Lee, and P.-K. Wei, "Enhancing detection sensitivity of metallic nanostructures by resonant coupling mode and spectral integration analysis," *Opt. Exp.*, vol. 22, no. 16, pp. 19621–19632, 2014.
[35] M. Das, D. Hohertz, R. Nirwan, A. G. Brolo, K. L. Kavanagh, and R. Gordon, "Improved performance of nanohole surface plasmon resonance sensors by the integrated response method," *IEEE Photon. J.*, vol. 3, no. 3, pp. 441–449, Jun. 2011.
[36] I. M. White and X. Fan, "On the performance quantification of resonant refractive index sensors," *Opt. Exp.*, vol. 16, no. 2, pp. 1020–1028, 2008.
[37] H.-P. Loock and P. D. Wentzell, "Detection limits of chemical sensors: Applications and misapplications," *Sens. Actuators B, Chem.*, vol. 173, pp. 157–163, Oct. 2012.
[38] C. Escobedo, "On-chip nanohole array based sensing: A review," *Lab Chip*, vol. 13, no. 13, pp. 2445–2463, 2013.
[39] M.-P. Murray-Méthot, M. Ratel, and J.-F. Masson, "Optical properties of Au, Ag, and bimetallic Au on Ag nanohole arrays," *J. Phys. Chem. C*, vol. 114, no. 18, pp. 8268–8275, May 2010.
[40] A. E. Cetin, D. Etezadi, B. C. Galarreta, M. P. Busson, Y. Eksioglu, and H. Altug, "Plasmonic nanohole arrays on a robust hybrid substrate for highly sensitive label-free biosensing," *ACS Photon.*, vol. 2, no. 8, pp. 1167–1174, Aug. 2015.
[41] K. Nakamoto, R. Kurita, O. Niwa, T. Fujii, and M. Nishida, "Development of a mass-producible on-chip plasmonic nanohole array biosensor," *Nanoscale*, vol. 3, no. 12, pp. 5067–5075, Dec. 2011.
[42] M. R. Rakhshani and M. A. Mansouri-Birjandi, "Engineering hexagonal array of nanoholes for high sensitivity biosensor and application for human blood group detection," *IEEE Trans. Nanotechnol.*, vol. 17, no. 3, pp. 475–481, May 2018.
[43] A. Lesuffleur, H. Im, N. C. Lindquist, and S.-H. Oh, "Periodic nanohole arrays with shape-enhanced plasmon resonance as real-time biosensors," *Appl. Phys. Lett.*, vol. 90, no. 24, Jun. 2007, Art. no. 243110.
[44] L. Pang, G. M. Hwang, B. Slutsky, and Y. Fainman, "Spectral sensitivity of two-dimensional nanohole array surface plasmon polariton resonance sensor," *Appl. Phys. Lett.*, vol. 91, no. 12, 2007, Art. no. 123112.
[45] J. Yuan et al., "Enhanced sensitivity of gold elliptic nanohole array biosensor with the surface plasmon polaritons coupling," *Opt. Mater. Exp.*, vol. 5, no. 4, pp. 818–826, 2015.
[46] E. N. Lazareva and V. V. Tuchin, "Measurement of refractive index of hemoglobin in the visible/nir spectral range," *J. Biomed. Opt.*, vol. 23, no. 3, 2018, Art. no. 035004.
[47] Y.-L. Yeh, "Real-time measurement of glucose concentration and average refractive index using a laser interferometer," *Opt. Lasers Eng.*, vol. 46, no. 9, pp. 666–670, Sep. 2008.

Tashfiq Ahmed (Member, IEEE) received the B.Sc. degree in electrical and electronic engineering (EEE) from the Bangladesh University of Engineering and Technology (BUET), Dhaka, Bangladesh, in 2021, where he is currently pursuing the M.Sc. degree.

He is currently working as a Lecturer with the EEE Department, BUET. His research interests include photonics, optoelectronics, plasmonics, and biosensors.

A. K. M. Naziul Haque received the B.Sc. degree in electrical and electronic engineering (EEE) from the Bangladesh University of Engineering and Technology (BUET), Dhaka, Bangladesh, in 2021.

He is currently working as a Lecturer with the CSE Department, Brac University, Dhaka. His research interests include nanophotonics, plasmonics, metamaterials, photonic inverse design, and quantum optics.

Muhammad Anisuzzaman Talukder joined the Electrical and Electronic Engineering Department, Bangladesh University of Engineering and Technology (BUET), Dhaka, Bangladesh, as a Lecturer, in early 2001, and has been serving as a Professor since 2014. He is also serving as the Director for the Research and Innovation Center for Science and Engineering, BUET. He also served at the University of Maryland, College Park, MD, USA, for several years as a Visiting Professor. He was with the University of Leeds, Leeds, U.K., from 2016 to 2018, as a Distinguished Marie-Curie Individual Fellow. He was an Honorary Fellow at the Hong Kong Polytechnic University, Hong Kong, from 2013 to 2015, and a Visiting Academic Fellow at the City, University London, London, U.K., in 2013.